computation

MDPI

Article

Buckling Assessment in the Dynamics Mechanisms, Stewart Platform Case Study: In the Context of Loads and Joints, Deflection Positions Gradient

Reza Hassanian [1,*,†] and Morris Riedel [1,2,†]

[1] The Faculty of Industrial Engineering, Mechanical Engineering and Computer Science, University of Iceland, 102 Reykjavik, Iceland; morris@hi.is
[2] Juelich Supercomputing Centre, 52428 Jülich, Germany
* Correspondence: seh@hi.is
† These authors contributed equally to this work.

Abstract: This study introduces an approach for modeling an arm of a Stewart platform to analyze the location of sections with a high deflection among the arms. Given the dynamic nature of the Stewart platform, its arms experience static and dynamic loads. The static loads originate from the platform's own weight components, while the dynamic loads arise from the movement or holding of equipment in a specific position using the end-effector. These loads are distributed among the platform arms. The arm encompasses various design categories, including spring-mass, spring-mass-damper, mass-actuator, and spring-mass-actuator. In accordance with these designs, joint points should be strategically placed away from critical sections where maximum buckling or deformation is prominent. The current study presents a novel model employing Euler's formula, a fundamental concept in buckling analysis, to propose this approach. The results align with experimental and numerical reports in the literature that prove the internal force of the platform arm is affecting the arm stiffness. The equal stiffness of an arm is related to its internal force and its deflection. The study demonstrates how higher levels of dynamic loading influence the dynamic platform, causing variations in the maximum arm's buckling deflection, its precise location, and the associated deflection slope. Notably, in platform arms capable of adjusting their tilt angles relative to the vertical axis, the angle of inclination directly correlates with deflection and its gradient. The assumption of linearity in Euler's formula seems to reveal distinctive behavior in deflection gradients concerning dynamic mechanisms.

Keywords: buckling; dynamic load; deflection; Stewart platform arm

Citation: Hassanian, R.; Riedel, M. Buckling Assessment in the Dynamics Mechanisms, Stewart Platform Case Study: In the Context of Loads and Joints, Deflection Positions Gradient. *Computation* **2023**, *11*, 227. https://doi.org/10.3390/computation11110227

Academic Editors: Shan Zhao, Martynas Patašius and Rimantas Barauskas

Received: 25 September 2023
Revised: 7 November 2023
Accepted: 13 November 2023
Published: 15 November 2023

1. Introduction

1.1. Evaluation and Context

Stewart platform is a parallel manipulator with applications across various fields [1]. The foundational concept of the Stewart platform can be traced back to Gough, who pioneered a parallel system that resembled a tire testing apparatus [2]. However, it was Stewart who first conceived the Stewart platform in 1965, with the specific goal of developing a flight simulator [3]. A wealth of literature discusses prototype designs and recommendations for designing and applying the Stewart platform. Merlet, for instance, details a large manipulator designed for mining operations [4]. One of Merlet's prototypes is utilized in ophthalmic surgery and at the European Synchrotron Radiation Facility (ESRF) [5]. As a stabilizer, the Stewart platform can mitigate rotational and damp linear motions [5]. It has various applications, such as stabilizing cameras [6], subterranean excavators [7], satellite positioning systems [8], and enhancing robotic platforms [4]. The Stewart platform design has been employed and developed by diverse industries, including aerospace, automotive, transportation, machine tool technology, and medical applications [5,9].

Merlet describes the main reason for interest in this platform as their impressive nominal load-to-weight ratio [4,10]. He designed a prototype platform weighing 35 kg that can effectively carry a load of 600 kg. Merlet's experimental study shows that the weight of the load is approximately equally distributed on all the arms [11]. Additionally, a notable advantage is that the stress experienced in each arm is in traction-compression, making it highly compatible with linear actuators and enhancing platform rigidity [11].

Merlet's definition characterizes a parallel manipulator as a "closed-loop mechanism in which the end-effector is connected to the base by at least two independent kinematic chains". Furthermore, he describes a fully-parallel manipulator as "a closed loop-manipulator with an n degrees-of-freedom (DOF) end-effector connected to the base by n independent chains, which have at most two links and are actuated by a unique prismatic or rotary actuator" [4,11]. The other definition in the literature realm is that parallel manipulators are generally classified into two primary categories: planar and spatial manipulators, depending upon their joints design [12]. Planar manipulators exhibit one to three degrees of freedom (DOF), while spatial manipulators are described as having three to six DOFs. Stewart platforms are categorized as parallel manipulators equipped with prismatic actuators and fall within the domain of spatial manipulators [12].

Among the previous works, there are different designs of connection configurations of the Stewart platform. However, there are three categories that have been tested experimentally and studied much more than others: the 6-6, 3-6, and 3-3 configurations [9]. The Stewart platform is composed of an upper plate (end-effector), and a lower plate (base) that are connected via the number of extendable arms connected through spherical or universal joints, and the configuration $I - J$ specifies how many joints are on the base plate and the end effector, respectively.

The Stewart platform achieves precise positioning and orientation adjustments by modifying the lengths of its arms [13]. An open research focus in the realm of the Stewart platform concerns its movement and structural framework [10,14]. The arm of the platform can be constructed using two or more elements within the platform's structure. As the arm of the Stewart platform operates through a linear actuator, insights from literature and existing prototypes reveal that the arm can be designed using configurations such as mass-spring, mass-spring-damper, mass-actuator (hydraulic or electric), or mass-spring-actuator [15,16]. These various configurations demonstrate the potential for constructing the platform arm using multiple interconnected parts. In this context, the platform arm's design is crucial, considering its fundamental nature as traction-compression and ensuring that joints are strategically not positioned to arm sections where critical stress and deflection occur.

Numerous initiatives have put forward mechanical analyses and models to define the stiffness of the elements constituting the arm of the Stewart platform, considering various configurations [17]. Moreover, utilizing the stiffness model can enhance and streamline the design of the platform [18]. Reports suggest that the arm elements' stiffness is influenced by fluctuations in internal arm forces [19].

1.2. Objective of This Research

The current study utilizes the column deflection concept in the mechanical analysis to propose a deflection model of the Stewart platform arm. In this context, the model provides insight into examining the critical sections of the arm with various Stewart platform boundary conditions. A Stewart platform with a 6-6 configuration that has six DOF, has been modeled. A loaded Stewart platform transits statics and dynamics forces to each arm. The statics force is related to the carried object by the end-effector, and the dynamics force is caused by the various positions of the end-effector and its movement.

This study has two main subjects: (i) investigating the assumption of disregarding $\frac{dy}{dx}$ in the buckling deformation formula [20] and illustrates that this assumption does not hold in the Stewart platform's arms as a dynamic mechanism, (ii) specifying the critical Stewart platform arm locations (with maximum deformation) to be considered in the arm design with multi-components and avoid the placement of the joint at a critical location.

The novelty of this study lies in identifying critical sections within dynamic arms (analogous to columns) that do not possess fixed, predefined locations. These results match the previous experimental works [17–19] that reported that the internal force of the platform arm is various, causing unfixed arm stiffness. It reveals that the critical deflection sections are not at fixed locations and is a function of dynamics parameters. This uncovers that the dynamic arm can exhibit critical deflection and stress at a range of the arm sections. The platform arm is assumed to be a column applying Euler's formula for buckling deflections [21–23] as a foundational tool and also aligned with Castigliano's theorem to find a deflection of the elastic structure [24]. This approach provides a transparent stream for designing the Stewart platform multi-element arm concerning the joints' location among the arm and not being at critical deflection sections. Moreover, the proposed model is capable of being useful to calculate arm stiffness. Consequently, the organizational framework of this work unfolds as follows: Section 2 expounds upon the methodology employed; Section 3 defines a numerical case study; Section 4 presents the obtained results; and finally, Section 5 encapsulates the derived conclusions.

2. Methodology

2.1. Theory

In the domain of six-degree-of-freedom Stewart platforms, there are three well-established joint configurations: the 6-6, 3-6, and 3-3. However, this study exclusively concentrates on the 6-6 configuration. In this particular setup, each arm is linked to the end-effector via a spherical joint and connected to the base through a universal joint. The theoretical framework used in this research is based on the following fundamental assumptions:

- The upper part exerts two different loads on the arms: a constant force due to its weight and a dynamic load that changes over time;
- Each arm has a segment with a uniform shape, without any joints or actuators;
- The deflection solution assumes that the tilt angle of the arms remains constant. (This assumption is valid because the solution is focused on a particular moment and is not dependent on time, making it reasonable to consider a fixed tilt angle.).

Based on the previously mentioned assumptions, Figure 1 illustrates the force components acting on the platform arm. To determine the deformation of the arm, this investigation utilizes Euler's Formula for Pin-end straight structures, tailored to match the boundary conditions specific to the platform arms. It must be noted that the load from the end-effector of the platform remains vertically oriented. The angular position of the platform arms, represented by the angle β, depends on both the applied load and displacement. This orientation can be clearly seen in Figure 1. It is important to emphasize that all arms maintain the same angle relative to the vertical orientation when the platform is stationary.

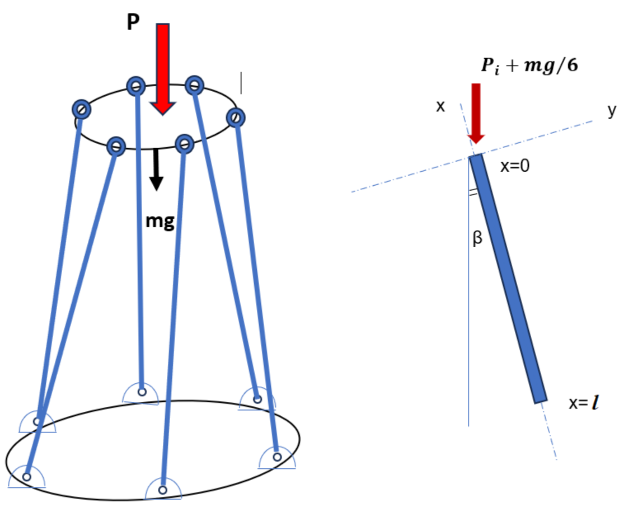

Figure 1. Illustrative depiction showcasing the schematic view of a 6-6 type Stewart platform.

To explore the consequences of the normal force and its impact on buckling, we apply the combined force onto an axis aligned with each arm's axial direction. This direction will be called the X axis, as shown in Figure 1. Perpendicular to the X axis is the Y direction, which is responsible for measuring buckling displacement. The total force component along the Y direction is transmitted through the spherical joint and does not affect buckling. Here, mg represents the weight of the upper platform, while the weight of the arm is denoted as $m_l g$, which is included in the overall force assessment. Based on the Merlet experiment report [11], this assessment assumes an equal distribution of force among the six arms, making P the driving (external/dynamic) load, which is then divided as $P_i = P/6$ for each platform arm. Demonstration of load distribution principles in Stewart platforms reveals that elevating the primary load (statics/dynamics) on the end-effector results in a larger internal load on each arm of the platform. This increased load directly influences both the buckling behaviors and the stiffness of the arms. However, the stiffness effects are not the subject of the present study. Based on the above-mentioned principles, the force acting on an individual arm, P_i is defined by Equation (1):

$$F = (P_i + mg/6 + m_l g)cos\beta, \tag{1}$$

In this equation, F represents the total axial force acting on the arm, and β represents the tilt angle between the arm and the vertical direction. Additionally, the weight of the arm produces a force component in the Y direction at the midpoint of the arm, which causes deflection. Following the boundary conditions of the arm, this deflection aligns with the principles outlined in reference [20]:

$$y_d = \frac{m_l g sin\beta}{48EI}(4x^3 - 3l^2 x), \tag{2}$$

Herein, y_d represents the deflection, g denotes the acceleration due to gravity, E stands for Young's modulus, and I denotes the moment of inertia. The parameter l defines the arm length, and x indicates the distance in the X orientation along the arm. According to Equation (2) the maximum deflection occurs at the midpoint of the arm ($x = \frac{l}{2}$), and it can be expressed as $y_d = \frac{m_l g l^3 \sin\beta}{48EI}$. This equation captures the relationship between the deflection (y_d), the arm weight ($m_l g$), arm length (l), tilt angle (β), Young's modulus (E), and moment of inertia (I).

Because of the interaction between the tilt angle and the applied forces on the platform arm, both weight-induced deflection and buckling of axial force occur. The overall deformation is the result of the combination of these deflection effects. The main equation acts as the governing rule for calculating the buckling response [20]:

$$\frac{\frac{d^2y}{dx^2}}{(1 + (\frac{dy}{dx})^2)^{\frac{3}{2}}} = \frac{-Fy}{EI}, \tag{3}$$

Equation (3) is a nonlinear differential equation where Euler's formula method could be used for the solution. This method is applied with the condition that $\frac{dy}{dx} \ll 1$, which has been allowed to disregard $\frac{dy}{dx}$. It is important to highlight that the present study will thoroughly investigate this assumption in Section 2.2, including illustrative examples for a more in-depth understanding. The validity of neglecting dy/dx in the linear assumption of buckling deformation will be assessed in a subsequent section. As will be demonstrated, this assumption does not appear to hold for the arms of the Stewart platform, which is a dynamic multi-degree of freedom mechanism. Following this approximation, the deflection caused by buckling could be calculated by solving Equation (4).

$$EI\frac{d^2y}{dx^2} = -Fy = -(P_i + mg/6 + m_l g)ycos\beta, \tag{4}$$

$$\frac{d^2y}{dx^2} + \frac{F}{EI}y = 0, \tag{5}$$

Considering the specified boundary conditions for the arm ($y_b(0) = y_b(L) = 0$), the resulting expression for the buckling deflection is outlined as follows:

$$y_b = asin\frac{\pi}{l}x, \tag{6}$$

As a result, by adding up the two deflections of the arm, which are denoted as y_d and y_b:

$$y_t = y_b + y_d = asin\frac{\pi}{l}x + \frac{m_l gsin\beta}{48EI}(4x^3 - 3l^2x), \tag{7}$$

In this equation, y_t represents the total deflection, while a is considered deterministic, signifying the maximum buckling deflection. This arises from the nature of differential Equation (3), which provides a simplified linear approximation derived from the main governing differential equation describing the behavior of an elastic curve [20].

It is important to emphasize that Equation (3) acts as an approximation that captures the linear aspects of the original equation governing curve deformation under elastic conditions. This approach simplifies and analyzes the system's response from a linear perspective, making it easier to understand the underlying mechanics. Nonetheless, it is essential to determine whether the slope is negligible or not, and Section 2.2 will thoroughly explore its implications.

2.2. Slope of the End of the Arm

The exclusion of $\frac{dy}{dx}$ in the Euler formula is justified by its smallness, which renders $(1 + (\frac{dy}{dx})^2)^{\frac{3}{2}} = 1$. In this study, the platform arm experiences two different types of deflection, as have been described above, which allows the investigation of the slope at the end of the arm, denoted as $\theta = \frac{dy}{dx}$, using Equations (2) and (6):

$$\theta_d = \frac{m_l gl^2 sin\beta}{16EI}, \tag{8}$$

$$\theta_b = a\frac{\pi}{l}, \tag{9}$$

$$\theta_{t,x=l} = \theta_b + \theta_d = a\frac{\pi}{l} + \frac{m_l gl^2 sin\beta}{16EI}, \tag{10}$$

Equation (10) offers evidence that supports the existence of a slope $\frac{dy}{dx}$ within the arm. This slope depends on various factors, including the arm length l, arm mass m_l, arm tilt angle β, Young's Modulus E, and moment of inertia I. It is important to note that the parameter a remains undetermined due to the linearity assumption in Equation (3). When solving the nonlinear equation, the response y_b yields two solutions with both real and imaginary components. The complex solution for y_b could help identify the omitted $\frac{dy}{dx}$ by distinguishing the real parts of these complex solutions.

The upcoming Section 3 and its results will numerically investigate the slope $\frac{dy}{dx}$. This investigation will involve presenting and discussing the slope within a deformed arm. These findings will be derived from finite element analysis (FEA) conducted using commercial software ANSYS, Inc., Canonsburg, PA, USA [25]. The numerical results of the current study will be compared to the Stewart platform arms that were investigated experimentally in the literature.

2.3. Critical Stress and Self-Bucking

Euler's pioneering work delved into the phenomenon of self-buckling, which arises from the weight of a column itself. This exploration resulted in the formulation of three influential papers (1778a, 1778b, 1778c) [21–23]. Over subsequent centuries, solutions to this problem have been refined [26–29]. However, in the current study, it is important to note that the arm's own weight causes deflection, introducing an axial component that enhances the buckling force. Moreover, the presence of various drivers, such as hydraulic or electric actuators in the Stewart platform arms, adds complexity. Some investigations also suggest incorporating mass and spring models, as mentioned in the introduction. These different arm types introduce variable loads on the arm, potentially leading to self-buckling depending on the mass and arm strength. It is crucial to emphasize that the load introduced by actuators or mass-spring models should be included in the external load calculation, which determines the arm's critical load. This critical load is determined based on the Euler formula solution for a pin-ended column [20]:

$$P_{cr} = \frac{\pi^2 EI}{l^2}, \tag{11}$$

here, P_{cr} represents the critical load. It is important to highlight that this solution is based on the assumption of $\frac{dy}{dx} = 0$ and utilizes the first frequency of the *Sine* solution for y_b. Through Equation (11), the critical load emerges as a function that is closely related to the material, geometry, and dimensions of the platform arm.

3. Case Study via Numerical Approach

The present study proposes a comprehensive model to study the deflection in a Stewart platform arm caused by a combination of loads from the end-effector, its own weight, and the applied driven load. This model was carefully constructed and thoroughly analyzed using the Ansys Inc. environment [20]. The solution is based on the FEA [30].

This model initially assumes the loaded arm's specific moment of motion, and the weight is placed on the end-effector. Then, it analyzes how the arm deforms under this load. This study explores various loads to understand the subtle effects of different load scenarios. This analysis helps pinpoint the critical areas where the arms experience the most deformation when they buckle. This information is vital for designing a reliable platform that incorporates components such as joints, mass, springs, and actuators. Furthermore, according to Euler's formula, it has delved into the often-overlooked aspect of the slope in buckling deflection. It has examined how this slope behaves in moving joints and mechanisms. This approach has provided a comprehensive understanding of how the existing slope influences dynamic systems of this kind.

The relevant dimensions and material properties of the FEA model have been listed in Tables 1 and 2. The material is a Steel Structure for the whole platform with properties captured from the 1998 ASME BPV Code, Section 8, Div 2, Table 5-110.1 [31]. The element type is Tetrahedrons (Tet10). Mesh quality metrics have aligned to the Skewness mesh style and have been used and maintained at a permissible range from 0 to 0.5. The span angle center in the meshing is set up as coarse. The meshing of the platform involved a total of 2531 elements and 6271 nodes for the final results with the specified level of accuracy. A uniform distributed load was applied to the end-effector for the structural simulation. To provide a comprehensive view of the distinct effects of different distributed loads and platform position, which leads to different load over time for each arm, this study ran the analysis three times, with uniform loads of 2 kPa, 3 kPa, and 4 kPa as the distributed load over the entire end-effector surface, respectively. The finite element analysis has converged, and it was examined with a few iterations and allowable change definitions of the Ansys software, ver. 2021 R2.

Table 1. The element sizes employed for generating the three-dimensional representation and finite element analysis of the Stewart platform within Ansys Inc., Canonsburg, PA, USA. [25].

Element Description	Value [Unit]
Arm Length	1230 mm
Arm Diameter	8 mm
Internal Height	1200 mm
End-Effector Diameter	600 mm
End-Effector Thickness	25 mm
Base Ring External Diameter	850 mm
Base Ring Internal Diameter	550 mm
Base Ring Thickness	30 mm

Table 2. The material characteristics incorporated for rendering the three-dimensional depiction and finite element analysis of the Stewart platform in Ansys Inc.

Properties	Value [Unit]
Density	7850 Kg/m^3
Young's Modulus	2×10^5 MPa
Poisson's Ratio	0.3
Bulk Modulus	1.66×10^5 MPa
Shear Modulus	7.69×10^4 MPa
Compressive Yield Strength	2500 MPa
Tensile Ultimate Strength	4600 MPa
Tensile Yield Strength	2500 MPa

In the current study, the Ansys software's ver. 2021 R2, adaptive convergence capability is used to attain the desired level of precision. Adaptive convergence, in this context, refers to the phenomenon where the system's response, such as stress or deformations, converges towards a consistent solution as the element size decreases in a well-defined model. Consequently, as adaptive convergence is achieved, the results cease to fluctuate with further mesh refinement, signifying that the prescribed numerical accuracy has been reached.

In practical mechanical engineering scenarios, precise or analytical solutions are often unattainable due to the intricate nature of materials, non-linear contacts, and non-linear deformations. Consequently, it becomes imperative to monitor relative accuracy, which is expressed as the percentage change in results between a coarser mesh and a finer mesh. Achieving adaptive convergence necessitates the iterative resolution of problems with varying levels of mesh discretization. This process typically commences with a coarser mesh and progressively advances to a more refined mesh. The relative accuracy can be defined in terms of *Relative error*, which is a comparison between the results from models with different mesh densities:

$$Relative\,error = 100(\frac{\phi_{i+1} - \phi_i}{\phi_i}) < \epsilon, \tag{12}$$

where ϕ is the quantity of the result (such as deformation or stress), subscript i denotes the refinement iteration, and ϵ is the user-specified accuracy.

Indeed, rather than relying on the potentially error-prone manual selection of refined meshes, Ansys facilitates the automated generation of these meshes for finite element analysis (FEA).

Importantly, the gravitational force's impact on the problem was considered and included in the analysis. The base ring was positioned as a fixed reference point to ensure model stability.

4. Results and Discussion

The present study conducted a comparative analysis between the analytical deflection and the actual numerical results, as explained in the theory section. Its results have been compared to the previous experimental studies and discussed to assess the model.

4.1. Platform Arm Deflection

The applied load on the FEA model with specified properties led to deflection. Figure 2 clearly illustrates the increase in the total arm deflection as the applied distributed load rises. This outcome aligns well with the observations from both Figures 2 and 3, effectively highlighting the significant occurrence of maximum deflection near the arm's midpoint. This alignment with Equation (7) was expected. The deformation pattern originates from the arm's connection with the top plate, reaching its peak deflection near the arm's midpoint. Additionally, an interesting trend emerges: higher load magnitudes result in a shift in the location of the total deflection, moving it from the middle section of the arm towards the upper segment. This observation aligns with the experimental findings reported by Adli et al. [19]. Adli et al. demonstrated that variations in deflection and stiffness occur in response to different internal forces applied to the platform arm. This finding is consistent with the finite element analysis (FEA) results presented by Li et al. [18], which emphasize the importance of incorporating platform arm deformation into the stiffness model.

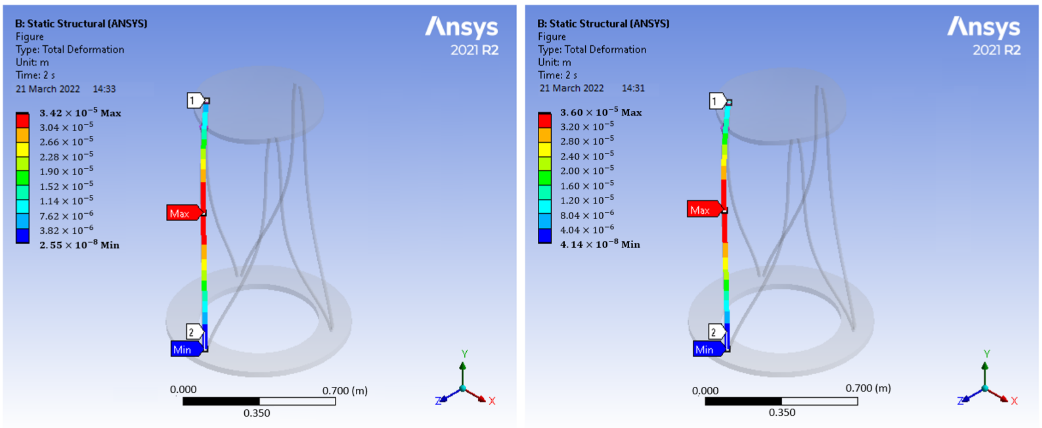

Figure 2. Visualization of Complete Deflection in a Platform Arm: On the left, a load of 2 kPa is applied, while on the right, the load is increased to 4 kPa. The uniform loading is directed onto the top plate, within the computational environment of Ansys Inc. [25].

In addition to the direct connection between higher internal loads and the increased deflections of the arm, the results display a trend of the maximum deflection location from the arm midpoint to the upper segment. This can be related to the neglected $\frac{dy}{dx}$ in the Euler formula assuming linearization of the nonlinear deformation equation, and it is evident in Figure 3.

Equation (10) demonstrates that the arm's slope is influenced by various variables, including the deterministic factor a, and its undetermined nature highlights its potential to affect the slope. Moreover, a crucial revelation emerges regarding Euler's formula, which assumed that $\frac{dy}{dx}$ was negligible, leading to the adoption of a linear equation for buckling deflection. However, it seems the significance of the slope $\frac{dy}{dx}$ in the platform arm design cannot be completely overlooked, especially when considering the dynamic arm's composition of components such as actuators, spring-mass systems, and the upper and lower arm segments. Different slopes at joint interfaces within the arm's structure can potentially lead to critical stress points and deflection.

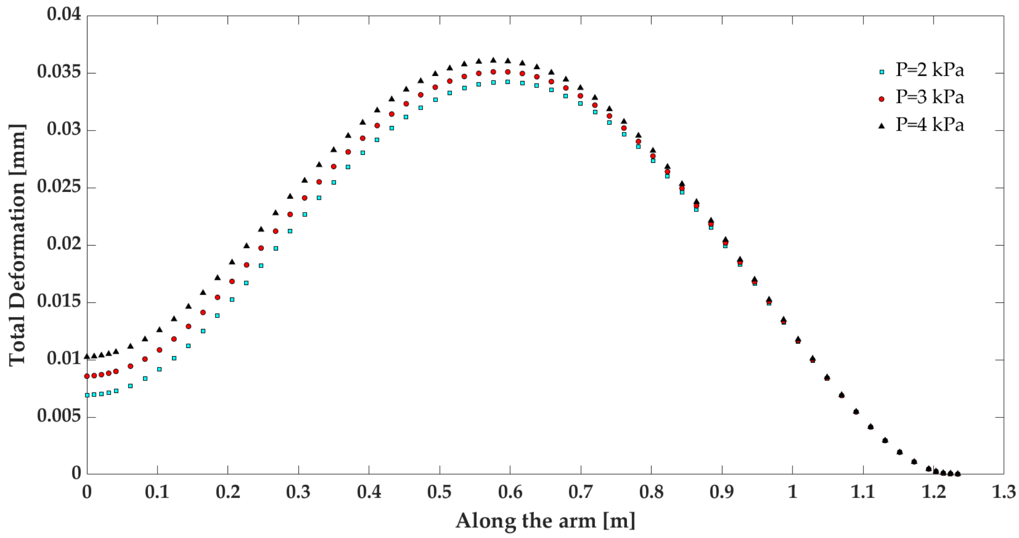

Figure 3. The visualization showcases overall deformation patterns within a true scale of the platform arm subjected to three distinct load configurations. Notably, based on Euler's formula for buckling deflection, it is expected to have the maximum deflection location in the middle of the arm, and it is not a function of the load. However, the result displays that when increasing the load over time, the maximum deflection location tends to be the upper half of the arm, and it is not a fixed location. Moreover, a discernible distinction is observed in the slope of the deflection function on both sides of the maximum displacement point.

Moreover, the Stewart platform often operates under dynamic loads, accompanied by variations in the arm's tilt angle over time. As widely recognized, the potential for fatigue failure due to dynamic forces requires increased attention, especially in regard to the arm's deflection-induced slope. The numerical solution presented here demonstrated that when the uniform distributed load was increased to 3 kPa and 4 kPa, the resulting maximum total deformation increased by 2.6% and 5.5%, respectively, compared to the 2 kPa pressure load.

4.2. Critical Buckling Stress

The stress analysis of the Stewart platform arm is illustrated in Figures 4 and 5. The internal force rises in the platform arm because of the increase in the distributed load corresponds to a rise in arm stress. This analysis notably identifies the middle section of the arm as a critical zone, displaying the highest stress concentrations. Specifically, the maximum stress within the Stewart platform arm increases by 17% and 35% when the uniformly distributed load applied to the end-effector is raised to 3 kPa and 4 kPa, respectively, compared to the 2 kPa pressure load. The insights gained from the stress analysis highlight the mid-length of the arm as a vulnerable area for potential maximum stress, with a pronounced tendency for deformation observed in the upper half of the arm.

In Figure 5, a noticeable trend becomes apparent: as the magnitude of the driven uniform distributed load increases, the location of maximum stress shifts towards the upper portion of the arm. This phenomenon aligns with the behavior of the buckling deflection slope, as discussed earlier, which matches the internal force and stiffness of the experimental reports [18,19]. The primary equation, Equation (3), for deflection, addressed under the assumption of linearity, appears to be a probable factor contributing to the observed change in the location of maximum stress, as discussed for the deflection results.

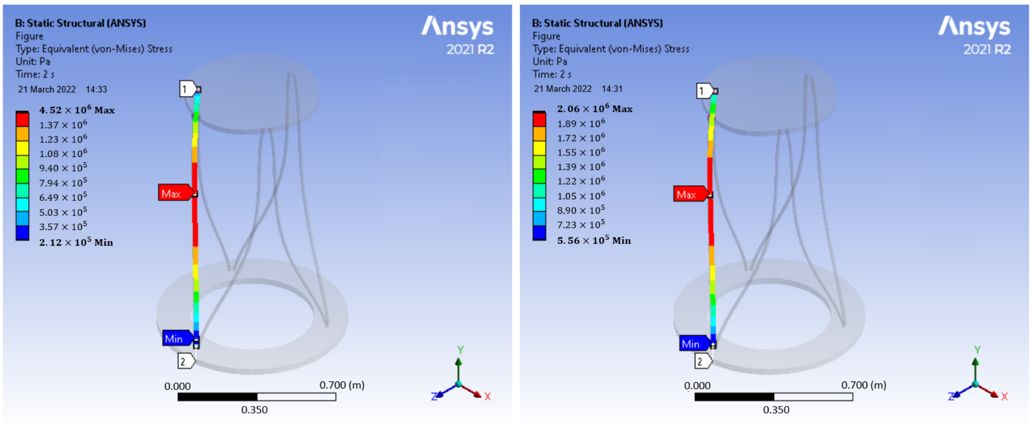

Figure 4. Presented here is an exhibition of the equivalent stress distribution across the true scale of the platform arm. On the left, a load of 2 kPa is applied, while on the right, the load is elevated to 4 kPa. The uniform load is uniformly distributed onto the end-effector within the computational framework of Ansys Inc. [25].

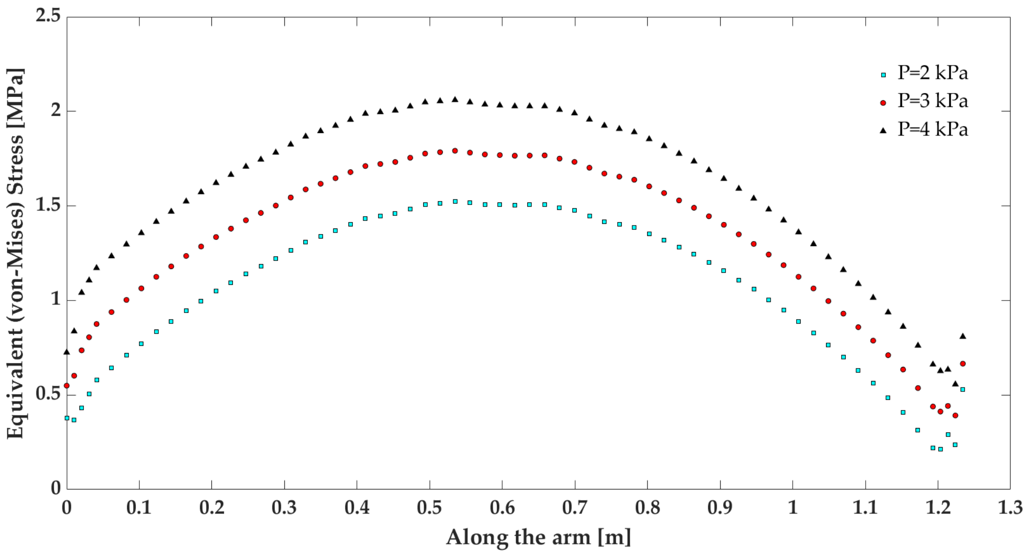

Figure 5. Illustrating the variation in equivalent stress along the length of a platform arm, this presentation encompasses three different loading scenarios. Notably, with similar behavior to the maximum deflection, the axial load of the arm depends on the tilt angle, and the dynamics load could be changed. It can be seen the critical stress location does not have a fixed location and, with extensive load, tends to the upper half of the arm, and it is not always in the middle of the arm as a buckling column with pinned-pinned boundary condition.

5. Conclusions

The current study proposes a model for the arm of the Stewart platform to examine and display its deflection caused by statics and dynamics load. An analytical investigation of the Stewart platform arm is defined based on the Euler formula concerning the platform boundary condition to assess the ignored dx/dy term effect of the buckling deformation equation for the multi-degree of freedom platform arm. Furthermore, a numerical case study of the platform has been simulated via finite element analysis and compared to experiments of the previous studies. The Stewart platform has different arm joint configurations, and this study investigated the type of 6-6. Each arm of the Stewart platform could be composed of two or more components. In most recommendation studies and prototypes, the platform arm has a design of mass-spring, mass-actuator, mass-damper-spring, and mass-spring-actuator structure. Concerning the available arm construction, the sub-part of the arm is connected via joints. Since the platform arm is a traction-compression element, the internal force leads to maximum stress and deformation in the arm section. Therefore, it is essential to recognize the critical sections with maximum stress or deflection and not place the joints in their location. Moreover, many studies have recently proposed a stiffness model for the platform arm to understand its deflection and stress and how it behaves with different internal forces. The results of the novel suggested model in this study aligned with the experimental reports of the Stewart platform arm internal force analysis and how it is related to stiffness and arm deflection. Additionally, the study represents that the critical section of the stress and deflection is not fixed, and it is proved and aligned with an experiment that reported the stiffness variation of the platform arm because of different internal loads. The location of the maximum deflection and stress could be defined. This capability makes it possible to figure out the critical sections' location and place the joints in the appropriate coordinate for multi-element arms with joints. Furthermore, in the Euler formula, the assumption for the linearity of the buckling equation ignored the buckling slope. However, it seems this gradient should be taken into attention for a column with dynamic loads, such as Stewart platform arms. The linearity inherent in Euler's formula results in a sine-based buckling deflection in the differential equation solution. However, the unaccounted slope within the differential equation adds complexity, giving rise to distinct slopes on either side of the maximum deflection point, which can be observed in dynamic mechanisms.

Author Contributions: R.H.: conceptualization, methodology, software, validation, formal analysis and writing—original draft. M.R.: methodology, writing—review and editing and supervision. All authors have read and agreed to the published version of the manuscript.

Funding: This work was performed in the Center of Excellence (CoE) Research on AI and Simulation-Based Engineering at Exascale (RAISE) and the EuroCC 2 projects receiving funding from EU's Horizon 2020 Research and Innovation Framework Programme and European Digital Innovation Hub Iceland (EDIH-IS) under grant agreement no. 951733, no. 101101903 and 101083762, respectively.

Institutional Review Board Statement: Not applicable.

Informed Consent Statement: Not applicable.

Data Availability Statement: Data are contained within the article.

Conflicts of Interest: The authors declare no conflict of interest.

References

1. Ng, C.C.; Ong, S.K.; Nee, A.Y.C. Design and development of 3–DOF modular micro parallel kinematic manipulator. *Int. J. Adv. Manuf. Technol.* **2006**, *31*, 188–200. [CrossRef]
2. Gough, V.E.; Whitehall, S.G. Universal Tyre Test Machine. In Proceedings of the 9th International Congress FISITA, London, UK, 30 April–5 May 1962; pp. 117–137.
3. Stewart, D. A Platform with Six Degrees of Freedom. *Proc. Inst. Mech. Eng.* **1965**, *180*, 371–386. [CrossRef]
4. Merlet, J.P. *Parallel Robots*; Springer: Dordrecht, The Netherlands, 2006. [CrossRef]
5. du Plessis, L.J. An Optimization Approach to the Determination of Manipulator Workspaces. Ph.D. Thesis, University of Pretoria, Pretoria, South Africa, 1999.
6. Gosselin, C.; Hamel, J.F. The agile eye: A high-performance three-degree-of-freedom camera-orienting device. In Proceedings of the 1994 IEEE International Conference on Robotics and Automation, San Diego, CA, USA, 8–13 May 1994; Volume 1, pp. 781–786. [CrossRef]
7. Arai, T.; Stoughton, R.; Homma, K.; Adachi, H.; Nakamura, T.; Nakashima, K. Development of a parallel link manipulator. In Proceedings of the Fifth International Conference on Advanced Robotics 'Robots in Unstructured Environments, Pisa, Italy, 19–22 June 1991; Volume 1, pp. 839–844. [CrossRef]
8. Jones, T.P.; Dunlop, G.R. Analysis of rigid-body dynamics for closed-loop mechanisms—Its application to a novel satellite tracking device. *Proc. Inst. Mech. Eng. Part I J. Syst. Control. Eng.* **2003**, *217*, 285–298. [CrossRef]
9. Brecht, D.K. A 3-DOF Stewart Platform for Trenchless Pipeline Rehabilitation. Master's Thesis, The University of Western Ontario, London, ON, Canada, 2015. Available online: https://ir.lib.uwo.ca/etd/3156 (accessed on 20 July 2023).
10. Dasgupta, B.; Mruthyunjaya, T. The Stewart platform manipulator: A review. *Mech. Mach. Theory* **2000**, *35*, 15–40. [CrossRef]
11. Merlet, J.P. Parallel manipulators: State of the art and perspectives. *Adv. Robot.* **1993**, *8*, 589–596. [CrossRef]

12. Snyman, J.A.; du Plessis, L.J.; Duffy, J. An Optimization Approach to the Determination of the Boundaries of Manipulator Workspaces. *J. Mech. Des.* **1998**, *122*, 447–456. [CrossRef]
13. Lazard, D.; Merlet, J.P. The (true) Stewart platform has 12 configurations. In Proceedings of the Proceedings of the 1994 IEEE International Conference on Robotics and Automation, San Diego, CA, USA, 8–13 May 1994; Volume 3, pp. 2160–2165. [CrossRef]
14. Furqan, M.; Suhaib, M.; Ahmad, N. Studies on Stewart platform manipulator: A review. *J. Mech. Sci. Technol.* **2017**, *31*, 4459–4470. [CrossRef]
15. Lu, Z.Q.; Wu, D.; Ding, H.; Chen, L.Q. Vibration isolation and energy harvesting integrated in a Stewart platform with high static and low dynamic stiffness. *Appl. Math. Model.* **2021**, *89*, 249–267. [CrossRef]
16. Jiang, M.; Rui, X.; Zhu, W.; Yang, F.; Zhang, J. Modeling and control of magnetorheological 6-DOF stewart platform based on multibody systems transfer matrix method. *Smart Mater. Struct.* **2020**, *29*, 035029. [CrossRef]
17. Svinin, M.; Hosoe, S.; Uchiyama, M. On the stiffness and stability of Gough-Stewart platforms. In Proceedings of the 2001 ICRA—IEEE International Conference on Robotics and Automation (Cat. No. 01CH37164), Seoul, Republic of Korea, 21–26 May 2001; Volume 4, pp. 3268–3273. [CrossRef]
18. Li, Y.W.; Wang, J.S.; Wang, L.P. Stiffness analysis of a Stewart platform-based parallel kinematic machine. In Proceedings of the 2002 IEEE International Conference on Robotics and Automation (Cat. No. 02CH37292), Washington, DC, USA, 11–15 May 2002; Volume 4, pp. 3672–3677. [CrossRef]
19. Adli, M.A.; Nagai, K.; Miyata, K.; Hanafusa, H. Analysis of Internal Force Effect in Parallel Manipulators. *Trans. Soc. Instrum. Control Eng.* **1991**, *27*, 1266–1273. [CrossRef]
20. Beer, F.; Johnston, E.; DeWolf, J.; Mazurek, D. *Mechanics of Materials*, 8th ed.; McGraw Hill: New York, NY, USA, 2019.
21. Euler, L. Determinatio onerum, quae columnae gestare valent. *Acta Acad. Sci. Petropolitanae* **1978**, *1*, 121–145.
22. Euler, L. Examen insignis puradoxi in theoria columnarum occurentis. *Acta Acad. Sci. Petropolitanae* **1978**, *1*, 146–162.
23. Euler, L. De Altitudine columnarum sub proprio pondere corruentium. *Acta Acad. Sci. Petropolitanae* **1978**, *1*, 163–193.
24. Castigliano, A. *The Theory of Equilibrium of Elastic Systems and Its Applications*; Dover Publications: New York, NY, USA, 1966.
25. *Ansys Workbench Teaching Version*; Ansys Inc.: Canonsburg, PA, USA, 2021.
26. Dinnik, A.N. *Buckling under Own Weight*; Don Polytechnical Institute: Rostov-on-Don, Russia, 1912; Volume 1, p. 19. (In Russian)
27. Willers, F.A. Das Knicken schwerer Gestänge. *ZAMM J. Appl. Math. Mech. Z. Angew. Math. Mech.* **1941**, *21*, 43–51. [CrossRef]
28. Engelhardt, H. Die Einheitliche Behandlung der Stabknickung mit Berücksichtigung des Stabeigengewichts in den Eulerfällen 1 bis 4 als Eigenwertproblem: (Exakte Lösungen, Näherungen nach Collatz und Gebrauchsformeln). Ph.D. Thesis, University of Münster, Münster, Germany, 1949.
29. Frisch-Fay, R. On the stability of a strut under uniformly distributed axial forces. *Int. J. Solids Struct.* **1966**, *2*, 361–369. [CrossRef]
30. Reddy, J.N. *An Introduction to the Finite Element Method*, 3rd ed.; McGraw Hill: New York, NY, USA, 2005.
31. American Society of Mechanical Engineers. *1998 ASME Boiler & Pressure Vessel Code*, 1998th ed.; ASME: New York, NY, USA, 1998.